NJC

PAPER

View Article Online
View Journal | View Issue

Cite this: *New J. Chem.*, 2016, **40**, 10161

Novel oxazine and oxazone dyes: aggregation behavior and physicochemical properties†

María N. Urrutia and Cristina S. Ortiz*

Received (in Montpellier, France) 5th July 2016,
Accepted 19th October 2016

DOI: 10.1039/c6nj02053d

www.rsc.org/njc

This research evaluated the synthesis and suitability of synthetic and commercial photosensitizers for use as potential photosensitizers in photodynamic therapy and photodynamic antimicrobial chemotherapy. Spectroscopic properties, experimental aggregation behavior in ethanol, *N*,*N*-dimethylformamide, water and water : polyethylene glycol 400, computational details, the ability to generate singlet oxygen, $\log P_{HPLC}$ and theoretical $\log P$ were determined. All the compounds evaluated formed aggregates in different media. Novel brominated tested compounds exhibited higher lipophilicity and generation of singlet oxygen in comparison with the corresponding starting reagent. The studies showed that the tested oxazine and oxazone dyes satisfy the conditions of a potential drug in terms of physicochemical and photochemical properties.

1. Introduction

Oxazines are an important group of organic dyes which constitute a widely used set of fluorescent stains in modern biology and histology with interesting photophysical and lasing properties.[1,2] These molecules are used as stains and imaging agents due to their high fluorescence quantum yield.[3]

Cresyl violet acetate (CV) is a member of the oxazine family of dyes that absorbs strongly in the red region, is photochemically stable and has a variety of applications as a microscopy stain. Long-lived excited states make this dye potentially useful as a photosensitizer in energy- and electron-transfer reactions.[4]

Cresyl red (CR), an impurity of commercial CV, was previously separated and purified, using preparative column liquid chromatography. This orange component is considered an oxazone (9-amino-benzo[α]phenoxazin-5-one) derived from the phenoxazonium salt by hydrolysis.[5]

Photodynamic therapy (PDT) and photodynamic antimicrobial chemotherapy (PACT) are technologies that utilize visible light and photosensitizers (PSs) to destroy cells.[6,7] These technologies can be defined as the systemic, local or topical administration of a non-toxic drug or dye known as a PS, which acquires the desired activity only when it is excited by light of an appropriate wavelength. PDT represents a well-established therapeutic modality, which was originally developed and approved for the treatment of a variety of solid tumors, while PACT emerged as a new treatment modality for bacterial infections due to its effectiveness and less likelihood of inducing bacterial resistance.[8,9] Photoactivation of a PS at the action site with light of a specific wavelength results in the destruction of specific cells by a complex cascade of chemical, biological and physiological reactions that occur after the formation of highly reactive species.[10,11]

Based on the above-mentioned research, the synthesis of novel oxazine and oxazone was addressed using pure CV and CR, cationic and neutral dyes, respectively. As the chemical structure of CV and CR permits the addition of substituents by aromatic electrophilic substitution using halogens, tribrominated cresyl violet ($CVBr_3$) and tribrominated cresyl red ($CRBr_3$) were synthesized. The chemical structures of these dyes are shown in Scheme 1. It has been reported that the introduction of heavy atoms into a molecule is a strategy to increase the efficiency of a spin-forbidden electronic transition from a singlet to a triplet state (intersystem crossing) and regulate the quantity of singlet oxygen ($^1O_2$) generation.[12,13]

The oxazine and oxazone molecules generally self-associate as many flat aromatic molecules. Although many of the physical properties of these dyes have been studied, little has been reported regarding any fine detail on the manner in which the self-association occurs.[3]

It is well known that the ionic dyes tend to aggregate in diluted solutions, leading to dimer formation, and sometimes to even higher-order aggregates.[14–16] The strength of dye aggregation is strongly dependent on the structure of the molecules, dye concentration, ionic strength, temperature and the nature of solvent. Aggregation may rise with an increase of dye concentration or ionic strength, but will decrease with rising temperature or the addition of organic solvents.[14,16]

Departamento de Farmacia, Facultad de Ciencias Químicas, Universidad Nacional de Córdoba, Haya de La Torre esq, Medina Allende, Ciudad Universitaria, X5000HUA, Córdoba, Argentina. E-mail: crisar@fcq.unc.edu.ar; Fax: +54-351-5353865; Tel: +54-351-5353865 int. 53356

† Electronic supplementary information (ESI) available. See DOI: 10.1039/c6nj02053d

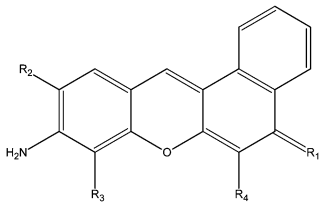

Dye	R_1	R_2	R_3	R_4
CV	$^{+}NH_2$	H	H	H
$CVBr_3$	$^{+}NH_2$	Br	Br	Br
CR	O	H	H	H
$CRBr_3$	O	Br	Br	Br

Scheme 1 Chemical structures of dyes.

It has been reported that the formation of aggregates in solution produces significant changes in the absorption and emission spectra, thus impairing the photochemical response and reducing the lifetimes of the excited state, most probably as a result of enhanced radiation, less excited state dissipation and lowering of the quantum yields of the excited states and of $^1O_2$ generation.[17–19]

In this work, we studied the effect of $CVBr_3$ and $CRBr_3$ concentration in different media on the aggregate formation and these results were compared with those obtained for CV and CR reference dyes under identical experimental conditions.[20,21]

Absorption UV-Vis spectroscopy and good monomerizing solvents were used for quantitatively studying the aggregation properties of dyes.[15,22–25] Besides, the experimental data were compared with theoretical calculations and the presence of monomeric species of CV and $CVBr_3$ was confirmed under the experimental conditions. The assays developed with CR and $CRBr_3$ indicated the absence of monomeric species.

In addition, the octanol–water partition coefficient for CR, $CVBr_3$ and $CRBr_3$ was determined by reversed-phase high-performance liquid chromatography (RP-HPLC) since this parameter plays an important role in the penetration of solutes into various biological membranes, tissues and barriers.[26,27] Also, the comparison between the experimental $\log P_{HPLC}$ and the calculated values, using different computer programs was included.

The efficacy of dyes to generate $^1O_2$ is considered a qualitative measure of their potential for increasing photoactivity.[28,29] Therefore, the capacity of the dyes to produce $^1O_2$ was determined.

The aim of this research was to determine the physicochemical characteristics of oxazine and oxazone dyes as potential PSs for PDT and PACT.

2. Results and discussion

2.1. Aggregation studies

The normalized spectral curves of CV in pure DMF recorded as a function of dye concentration (3.11×10^{-6}–5.60×10^{-5} M) are shown in Fig. 1. The dye showed an absorption band at 482 nm, and at the different evaluated concentrations, it was overlaid and obeyed the Lambert–Beer law. Therefore, the analysis of the results suggests that one species is present under these experimental conditions. According to the literature, DMF is a solvent that favors the monomeric species in solution.[22,30] An interesting observation was that the shape of the absorption spectra was not modified in the concentration range studied.

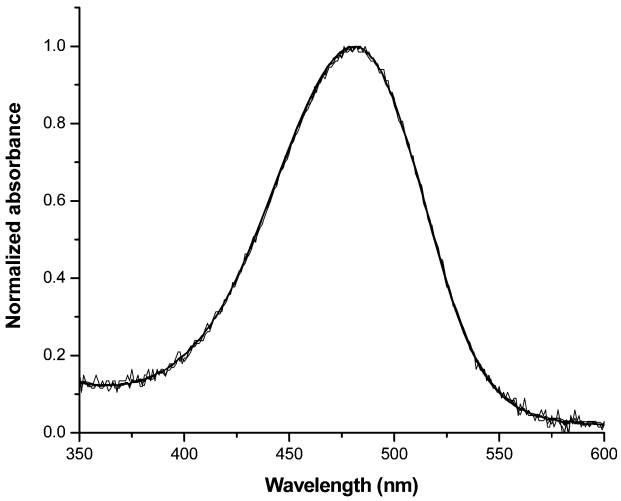

Fig. 1 Normalized absorption spectra of CV in DMF as a function of concentration at 482 nm, n = 10. [CV] = 3.11×10^{-6}–5.60×10^{-5} M.

The increase of the dye concentration in solution led to an increase in the absorbance; however, a new band did not appear. Furthermore, the band at 482 nm was assigned to the monomeric form of CV.

The normalized absorption spectra of CV at 602 nm in pure ethanol as a function of dye concentration (3.11×10^{-6}–4.67×10^{-5} M) presented spectral curves that were almost overlaid (Fig. 2). The dye exhibited one absorption band at 602 nm with a very weak shoulder at approximately 480 nm. The absorption band and the shoulder appeared even at the lower concentrations evaluated. The absorption maximum at 602 nm was assigned to the aggregate form of the dye and the shoulder at 480 nm to the monomeric species.

Aggregation of ionic dyes will be possible if there are certain very strong attractive interactions, which first of all overcome the Coulombic repulsion and then bring the component molecules to a reasonable distance to form dimers and subsequently higher aggregates. The geometry of the dimer in solution, the inclination of the component molecules in the dimer as well as their minimum distance of approach are of great significance to understand the roles of hydrophobic interaction and the steric factor in such aggregate formation.[14]

In this experimental case, a band of an aggregate form of the dye with a maximum absorption wavelength of around 602 nm was observed when using ethanol. This species was predominant in all the concentration ranges studied. The band

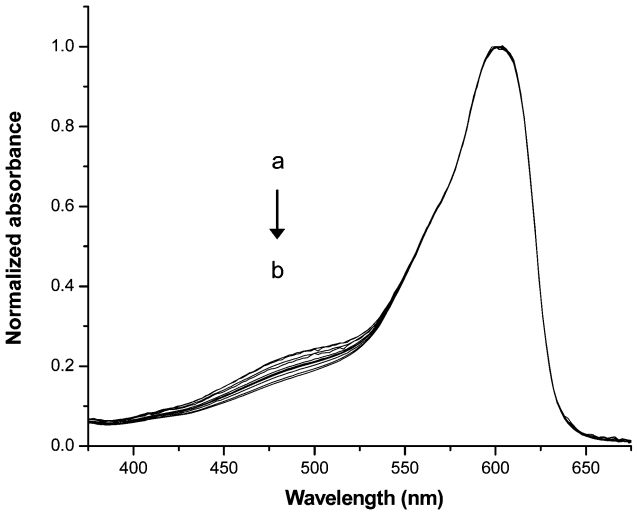

Fig. 2 Normalized absorption spectra of CV in ethanol as a function of concentration at 602 nm using 1 cm path length quartz cells, n = 11. [CV] (a) 3.11×10^{-6} M; (b) 4.67×10^{-5} M.

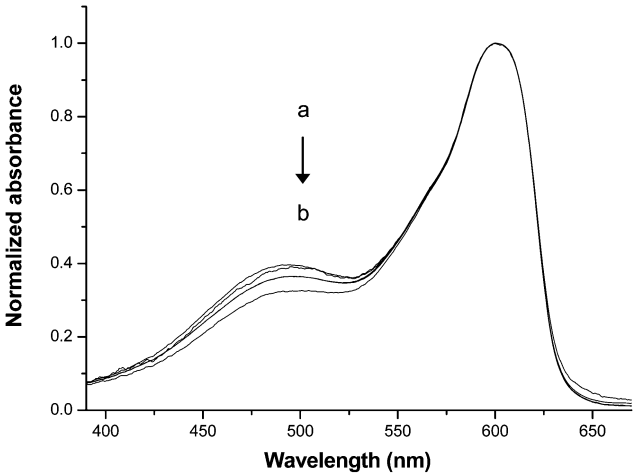

Fig. 3 Normalized absorption spectra of CV in ethanol as a function of concentration at 601 nm using 5 cm path length quartz cells, n = 5. [CV] (a) 6.22×10^{-7} M; (b) 3.11×10^{-6} M.

assigned to the monomer species decreased with the increase of the dye concentration related to the aggregated band.

In order to confirm the monomer assignation in ethanol, the other experience was developed in the same solvent employing 5 cm path length quartz cells and solutions of lower dye concentration (6.22×10^{-7}–3.11×10^{-6} M) with the objective of observing a more pronounced weak band (Fig. 3). These spectral curves showed a well-defined shoulder at approximately 480 nm, which confirmed our assignation. The monomer species was evident and strong in all spectral curves and the normalized absorption spectra were almost overlaid.

In order to deepen the study of aggregation of CV dye, the compound was assayed in different DMF : ethanol mixtures. The absorption spectra are shown in Fig. 4. In these studies, the concentration of the chosen dye was 1.87×10^{-5} M due to the

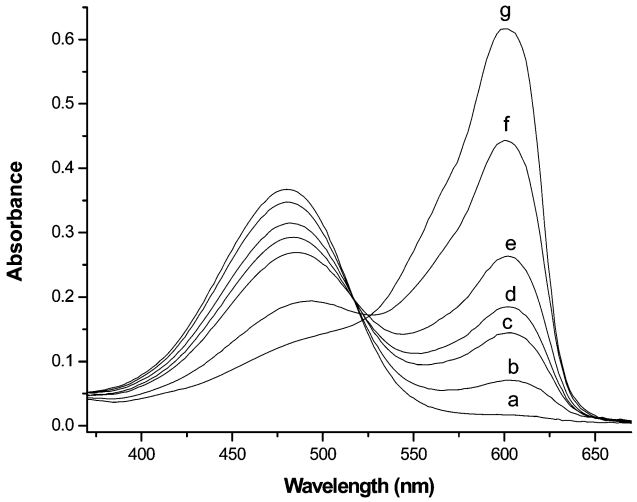

Fig. 4 Changes in UV-Vis spectra of CV at 1.87×10^{-5} M in DMF with an increasing amount of ethanol in the solution. Proportions of DMF : ethanol v/v: (a) 100 : 0; (b) 87.5 : 12.5; (c) 75 : 25; (d) 62.5 : 37.5; (e) 50 : 50; (f) 25 : 75; (g) 0 : 100.

optimal absorbance of the monomer and aggregate species. The addition of increasing amounts of ethanol to DMF gradually decreased the absorption maximum band at 480 nm in pure DMF (monomer) and increased the absorption band at 602 nm in pure ethanol (aggregate). As noted earlier, the shapes of the absorption spectra of CV in pure DMF (Fig. 1), pure ethanol (Fig. 2 and 3) and DMF : ethanol mixtures (Fig. 4) were different. These assays revealed that only the monomer was detectable in pure DMF, while the aggregate was not observed in that solvent. In general, dyes aggregate more strongly in ethanol than in DMF, which is known as a good monomerizing solvent that increases the quantity of monomers in solution.[22,30] This can be explained considering that the strength of aggregation between two or more dye molecules depends on the structure of the dye, the solvent and the presence or absence of electrolytes.[14–16]

However, the band of the aggregate centered at around 602 nm and the very weak shoulder at 480 nm attributed to the monomer form were observed at higher ethanol proportions. Therefore, these studies suggest that higher ethanol proportions decrease the absorbance at 480 nm and increase the aggregate band.

Different kinds of interactions between molecules, such as van der Waals, intermolecular hydrogen bonding and hydrogen bonding with the solvent could also explain the aggregation behavior. In fact, various mechanisms have been suggested to explain the forces holding dye ions together in solution, so it is necessary to point out that for a given dye/solvent system, more than one mechanism may be important.[20] To form the simplest aggregate, the dimer, the dye–dye interaction should be strong enough to overcome any other forces which would favor the solvation of the monomer.[31]

Generally, the aggregate formation is inhibited by organic solvents, and even more so by PEG 400, which is considered a good monomerizing solvent.[4,20,24,25,32] Therefore, the behavior of CV as a function of dye concentration was analyzed in

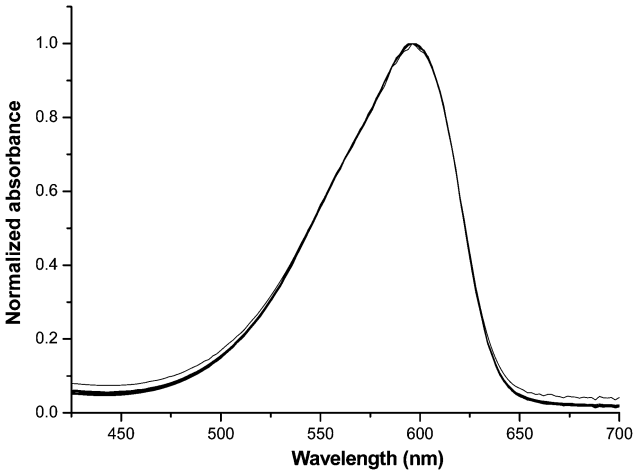

Fig. 5 Normalized absorption spectra of CV in PEG400 : water mixture (25 : 75 v/v) as a function of concentration at 596 nm, n = 10. [CV] = 3.11×10^{-6}–4.36×10^{-5} M.

PEG 400 : water 25 : 75 v/v (Fig. 5). The aggregate of the dye was the only species in solution, and responsible for the band at 596 nm. Furthermore, the normalized absorption spectra of all the spectral curves at 596 nm were found to be overlaid and obeyed the Lambert–Beer law in the concentration ranges studied (3.11×10^{-6}–4.36×10^{-5} M).

These assays allowed corroborating the assignation of monomer and aggregate bands of CV dye in different solvents and as a function of dye concentration.

Also, the CV dye in aqueous solutions was investigated to compare our results with the published data in the literature.[2,4,33,34] The normalized absorption spectra of this dye at different concentrations (3.11×10^{-6}–5.60×10^{-5} M) in aqueous solution were analyzed and are shown in Fig. 6. The dye exhibited an absorption band at 586 nm, with a shoulder at approximately 550 nm, and both appeared even at very low concentrations and increased as a function of dye concentration in the solution. The aggregate of the dye was the predominant species, and responsible for the principal band at 586 nm. The increase of the dye concentration produced a more pronounced increase of the weak shoulder in comparison with the band at 586 nm, so the principal band was assigned to the aggregated species of CV, while the shoulder was assigned to higher aggregates. The presence of aggregates was indicated by the isosbestic point at 510 nm. Since the spectral changes upon aggregation are dependent on the properties of the isolated molecule, the degree of spectral changes is not a direct indication of the degree of aggregation.[35]

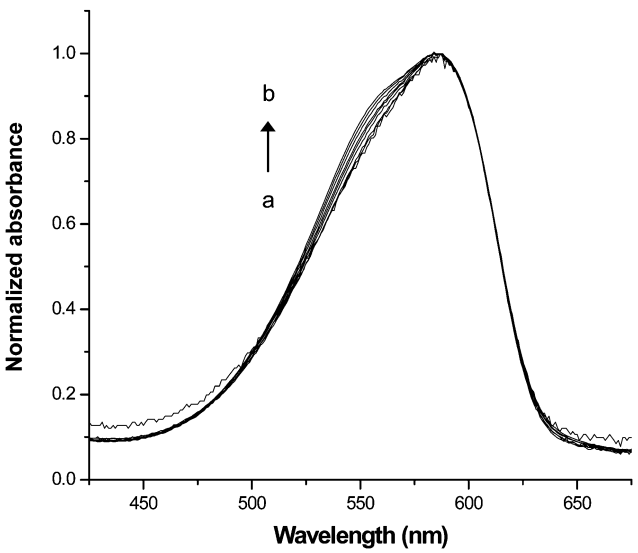

Fig. 6 Normalized absorption spectra of CV in aqueous solution as a function of concentration at 586 nm, n = 10. [CV] (a) 3.11×10^{-6} M; (b) 5.60×10^{-5} M.

The new dye $CVBr_3$ was evaluated in pure DMF and showed an absorption band at 474 nm in the concentration range analyzed (1.79×10^{-6}–3.23×10^{-5} M), which was assigned to the monomeric species. The normalized spectral curves revealed that the monomeric band was overlaid (ESI,† Fig. S1). The same tendency was observed when the CV normalized absorption spectra in DMF (Fig. 1) were compared with the corresponding normalized absorption spectra of the new derivative (ESI,† Fig. S1). Both dyes showed one band attributed to the monomeric form of the compound.

Besides, the new dye was evaluated as a function of concentration (1.79×10^{-6}–3.23×10^{-5} M) in ethanol (Fig. 7). An absorption band at 474 nm which was assigned to the monomeric species, could be observed at low dye concentrations, but as the concentration of $CVBr_3$ increased, a second band at a higher wavelength appeared. This dye existed only as a monomer in ethanol at concentrations lower than 1.43×10^{-5} M and the new band at 594 nm became greater than the monomer band when the dye concentration was $\geq$ than 3.23×10^{-5} M.

In the concentration range studied, the Lambert–Beer Law was not obeyed and the appearance of a new band was rationalized in terms of dye aggregation.[16,31] The concentration dependence of $CVBr_3$ in ethanol resulted in a bathochromic aggregate band (J-band), so the spectra of the aggregate were red-shifted with respect to the monomeric form. These kinds of aggregates are called J-aggregates.[17,36]

The $CVBr_3$ aggregate formation in ethanol was observed at higher concentrations ($>1.79 \times 10^{-5}$ M) in comparison with CV ($>3.11 \times 10^{-6}$ M), which indicates that in this solvent there were significant differences as a consequence of the presence of three bromine atoms. One of the possible explanations for these great differences in aggregation between CV and $CVBr_3$ is that the bromine atoms prevented molecular aggregation because they are bulky substituents. Therefore, the steric hindrance may have inhibited aggregation among the dye units, which resulted in a weak aggregation. It has been previously reported that aggregation of some PSs in organic solutions can be suppressed by peripheral substitution with long alkyl chains or bulky substituents.[37] Several authors have confirmed that bulky lipophilic substituents ensure good monomerization. One of them has found that the *tert*-butyl group inhibits dimerization more than long alkyl chains.[38,39]

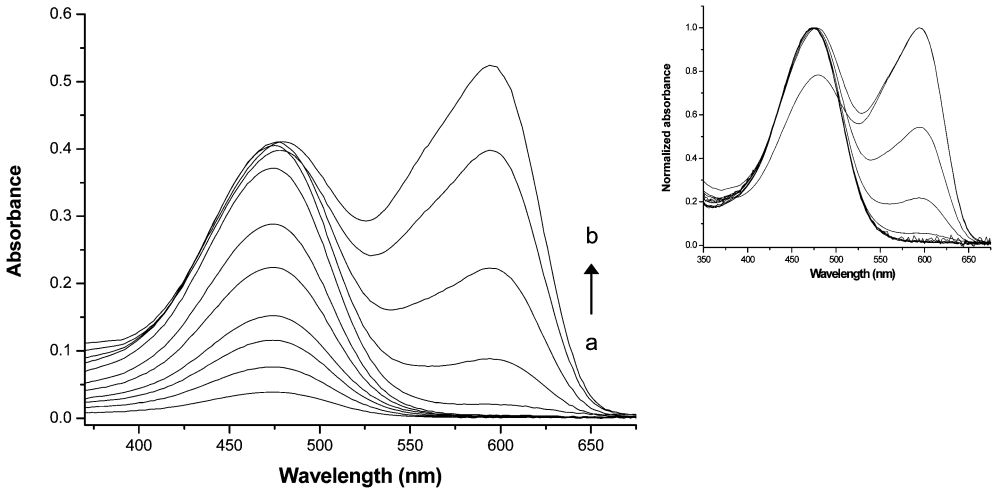

Fig. 7 Absorption spectra of $CVBr_3$ at different concentrations in ethanol. [$CVBr_3$] (a) 1.79×10^{-6} M; (b) 3.23×10^{-5} M. Inset: Normalized absorption spectra as a function of dye concentration.

It can be concluded that the introduction of a bulky substituent enhances the lipophilic character of CV, and prevents molecular aggregation due to a steric reason, potentially resulting in better photochemical and photophysical characteristics that could improve the PDT properties.[40,41]

Halogens can modify the electronic properties of the dyes because of the resonance effects. This has been widely studied in copper and zinc phthalocyanines replaced by electronegative fluorine and chlorine atoms. The differences observed could be attributed to the changes in the distribution of p-electrons due to mesomeric and/or inductive effects. In addition, the molecular structure of dyes and their environment can strongly influence the point charge effect, which consequently affects their photophysical properties.[42]

The lower aggregation of the new derivative $CVBr_3$ is a very significant result because the aggregation phenomenon shortens the triplet-state lifetimes and reduces the singlet oxygen quantum yield.[38] In addition, from a biological viewpoint, it was expected that the new compound compared to the starting reagent would predominate as monomers (active form) in cell membranes, so this could be a better PS in PDT and PACT.

On the other hand, CR was studied as a function of dye concentration (10^{-5}–10^{-4} M) in DMF and ethanol, showing an absorption band at 514 nm and 520 nm, respectively (ESI,† Fig. S2). The novel derivative, $CRBr_3$ was evaluated in DMF and ethanol as a function of dye concentration (10^{-5}–10^{-4} M) (ESI,† Fig. S3). These experiences demonstrated the same tendency for both dyes. The tribrominated derivative showed a single band at 502 nm in DMF and at 498 nm in ethanol, which was assigned to the aggregated species because CR and $CRBr_3$ dyes are neutral and molecular structures without a charge tend to aggregate at low concentrations in comparison to charged compounds.[14,43,44] Besides, the results obtained even at higher concentrations showed a unique band in ethanol, which is responsible for the increase in the aggregation tendency in comparison with DMF.[15,16]

The assignments for the four dyes were confirmed by theoretical calculations in DMF and compared with the experimental UV-vis spectra in DMF and ethanol. The maximum absorption was calculated after initial geometry optimization.

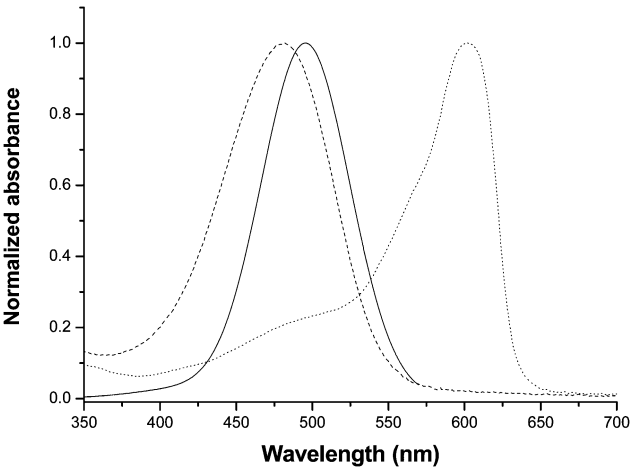

Fig. 8 Theoretical and experimental visible absorption bands for CV. Solid-line: theoretical spectrum of the monomer in DMF (λ_{ES} = 495.5 nm); dashed-line: experimental spectrum of the monomer in DMF (λ_{Exp} = 482 nm); dotted-line: experimental spectrum of the aggregate in ethanol (λ_{Exp} = 602 nm).

Fig. 8 shows the experimental visible absorption band (λ_{Exp}) and the simulated excited-state (λ_{ES}) of CV in DMF (monomer) and in ethanol (aggregate). It could be observed that the experimental monomeric band and the theoretical band did not show a significant difference, but the difference between the aggregate band in ethanol (dotted line) and the theoretical band (solid-line) is clearly evident.

The theoretical and experimental bands for the monomer of $CVBr_3$ in DMF and the experimental band for the aggregate in ethanol are shown in Fig. 9. The bands in DMF presented a unique band without significant differences in the maxima wavelength. This monomeric assignation was corroborated with the experimental spectrum in ethanol which showed two bands attributed to monomer (λ_{max} = 474 nm) and aggregate species (λ_{max} = 594 nm).

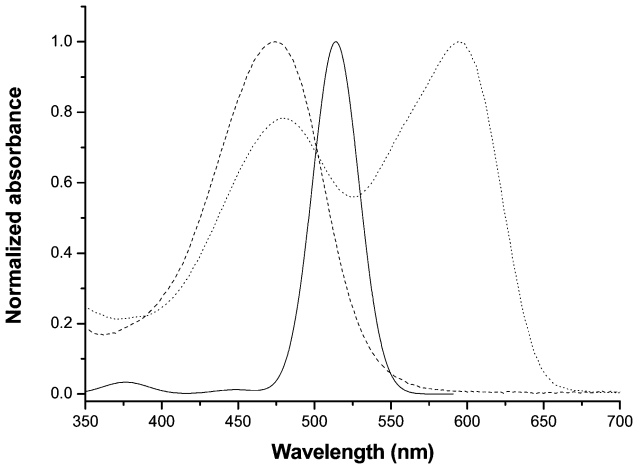

Fig. 9 Theoretical and experimental visible absorption bands for $CVBr_3$. Solid-line: theoretical spectrum of the monomer in DMF (λ_{ES} = 513.9 nm); dashed-line: experimental spectrum of the monomer in DMF (λ_{Exp} = 474 nm); dotted-line: experimental spectrum of the aggregate in ethanol (λ_{Exp} = 594 nm).

The theoretical band in DMF and the experimental visible band in DMF and ethanol of CR and $CRBr_3$ are shown in ESI,† Fig. S4 and S5, respectively.

The maximum absorption bands calculated for the monomer and the maximum experimental aggregate form in DMF and ethanol for both dyes revealed a significant difference among them and confirmed the assignment given to them.

Comparison of the UV-visible spectra and the calculated spectra for CV and $CVBr_3$ indicated that the general shape was similar and the shift was not significant, considering that the same calculation methodology was applied and the data were sufficiently close to the experimental results. Similar variations between experimental and calculated spectra have also been reported for other compounds.[45,46] In addition, the experimental UV-visible spectra in DMF with the calculated spectra for CR and $CRBr_3$ showed significant differences, which supports the assignation given under the evaluated conditions.

The results obtained indicate that the strength of aggregation largely depends on the structure of the dye molecule.

2.2. Determination of log *P*

2.2.1. $\log P_{HPLC}$. The correlation between the $\log k'$ values and the composition of the mobile phase (φ between 65% and 90%) was established using the reference compounds (Material Details, eqn (3)), and showed a linear relationship, as can be seen in Table 1. In this experimental cases, it is possible to note that the slope is negative when it is related to the hydrophobic surface of the molecule which interacts with the non-polar stationary phase.[30] The $\log k_w$ values for all compounds were calculated and the correlation between these data and $\log P_{O/W}$ for the reference compounds was expressed by eqn (1) with an excellent fit.

$$\log P_{O/W} = (0.84 \pm 0.03) \log k_w + (1.0 \pm 0.1) \quad (1)$$

$$n = 7;\ r = 0.99576;\ r^2 = 0.99154;\ s = 9.86457;\ F = 704.35$$

For all compounds, $\log P_{HPLC}$ values were calculated according to eqn (2) and the values are shown in Table 1.

$$\log P_{HPLC} = (0.84 \pm 0.03) \log k_w' + (1.0 \pm 0.1) \quad (2)$$

The $\log P_{HPLC}$ values obtained for CV, $CVBr_3$, CR and $CRBr_3$ were compared. The lipophilicity was increased for solutes with electron-withdrawing bromine substituents. The lipophilic parameter of a drug candidate seems to be the most important physicochemical parameter in the structure–activity relationship studies because it has been shown that an increase in lipophilicity leads to increased cellular uptake, which is usually correlated with increased biological activity.[26,47,48]

2.2.2. Theoretical calculation clog *P*. Comparison of the experimentally measured $\log k_w$ and computer estimated lipophilicity parameters revealed a good linear correlation for the set of evaluated compounds (Material details, eqn (4)). The parameters and statistical data of correlation between $\log k_w$ and clog *P* values are shown in Table 2.

The highest correlation, which was satisfactory, was obtained using the OSIRIS program. A good linear correlation was also obtained, using milog *P* and ACD/log *P*, with *r* values from 0.913 to 0.870, according to the accepted criteria from the literature.[49]

Table 1 Determination of $\log P_{HPLC}$ values

Compounds	λ_{max}[a] (nm)	$\log P_{O/W}$[b]	φ	*S*	$\log k_w$[c]	*r*	$\log P_{HPLC}$
Ref.							
Cresyl violet	590	2.83	65–85	−0.031 ± 0.002	2.3 ± 0.1	0.98734	2.9 ± 0.1
Neutral red	540	3.20	65–85	−0.033 ± 0.002	2.6 ± 0.1	0.99066	3.2 ± 0.1
Phenanthrene	280	4.52	70–90	−0.044 ± 0.005	4.2 ± 0.4	0.95620	4.5 ± 0.4
Anthracene	250	4.56	70–90	−0.046 ± 0.003	4.4 ± 0.2	0.98614	4.7 ± 0.2
Crystal violet	590	4.95	65–85	−0.060 ± 0.005	4.8 ± 0.2	0.97428	5.0 ± 0.2
9-Bromo-phenantrene	280	5.45	70–90	−0.052 ± 0.004	5.1 ± 0.3	0.97879	5.3 ± 0.3
Rose bengal	550	6.58	65–90	−0.083 ± 0.003	6.8 ± 0.2	0.99362	6.7 ± 0.3
Test substances							
$CVBr_3$	590	—	75–90	−0.0445 ± 0.0009	4.21 ± 0.07	0.99889	4.5 ± 0.1
CR	510	—	65–90	−0.038 ± 0.002	3.2 ± 0.1	0.99081	3.7 ± 0.1
$CRBr_3$	510	—	70–90	−0.053 ± 0.005	5.3 ± 0.4	0.96813	5.5 ± 0.4

[a] In mobile phase of RP-HPLC. [b] Literature data. [c] n = 3.

Table 2 Parameters and statistical data of correlation between log k_w and clog P values

	a	b	r	s	F
OSIRIS	1.6 ± 0.2	−2.1 ± 0.8	0.913	2.925	74.053
milog P	1.4 ± 0.2	−1.4 ± 0.8	0.892	3.164	58.775
ACD/log P	1.8 ± 0.3	−2 ± 1	0.870	5.681	47.887

a: slope; b: intercept; r: r-square; s: residual sum of squares; F: value of the fisher test of significance.

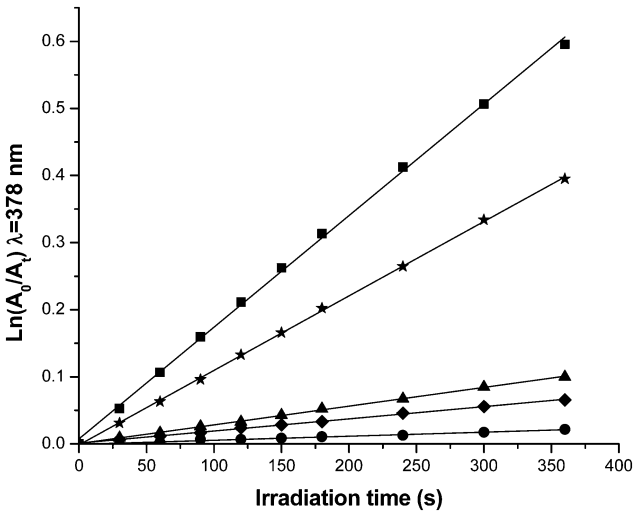

Fig. 10 First-order plots for photooxidation of DMA photosensitized by MB (square), CV (circle), $CVBr_3$ (rhombus), CR (triangle) and $CRBr_3$ (star) in DMF.

2.3. Photodynamic properties: singlet oxygen determination

Fig. 10 shows the semilogarithmic plots describing the progress of the reaction for DMA in DMF photosensitized by MB, CV, $CVBr_3$, CR and $CRBr_3$. The values of the observed rate constant (k_{obs}) were obtained and Φ_Δ values were calculated using eqn (6) (Table 3).

A higher efficiency in $^1O_2$ production was determined for $CVBr_3$ and $CRBr_3$ in comparison with the corresponding starting reagent. This could be explained in terms of the heavy-atom effect. The value of $CRBr_3$ was higher than that of $CVBr_3$ due to the carbonyl group that increased the Φ_Δ value.[50]

The experimental results have demonstrated that new derivatives of the oxazine and oxazone family were obtained with a high grade of purity. The novel derivatives have proved to have better photochemical and lipophilic properties than the commercial dyes.

Table 3 Kinetic parameters for photooxidation of DMA in DMF sensitized by the studied PS and singlet oxygen quantum yield (Φ_Δ)

Dye	k_{obs} ($\times 10^{-5}$; s^{-1})	Φ_Δ[a]
Methylene blue	166 ± 2	1
CV	6.0 ± 0.3	0.04
$CVBr_3$	18.2 ± 0.2	0.11
CR	27.9 ± 0.2	0.17
$CRBr_3$	111.0 ± 0.7	0.65

[a] Relative to methylene blue.

3. Conclusions

Various photosensitizers (PSs) have been clinically approved for the treatment of several malignant and non-malignant diseases. Most of them are hydrophobic and can aggregate very easily in aqueous media which can affect their photophysical, chemical and biological properties. Therefore, the aggregation behavior and physicochemical and photodynamic properties of cresyl violet acetate (CV) and cresyl red (CR) and the novel derivatives tribrominated cresyl violet ($CVBr_3$) and tribrominated cresyl red ($CRBr_3$) were studied.

By analyzing the effects of solvents on the spectral properties of the four dyes, we demonstrated that substitution in the molecule, different solvents and dye concentrations have a great influence on the aggregation behavior. The novel bromine derivative (tribrominated cresyl violet ($CVBr_3$)) formed aggregates at much higher concentrations in comparison with its precursor, which was associated with the bromine substituent.

The lipophilic parameter of the newly synthesized tribrominated cresyl violet ($CVBr_3$) and tribrominated cresyl red ($CRBr_3$) determined by RP-HPLC showed a good correlation with the theoretical calculations. The tribrominated dyes presented a higher lipophilicity in comparison with cresyl violet (CV) and cresyl red (CR). It has been reported that high lipophilicity is related to the efficacy of the compounds, which is an important requirement for high activity.

On the other hand, the results obtained confirmed the hypothesis that the singlet oxygen quantum yield increases due to halogenation in structurally related molecules. This is in agreement with the expected effects of heavy atoms on the spin–orbit coupling between the singlet and triplet states.

In conclusion, the novel compounds tribrominated cresyl violet ($CVBr_3$) and tribrominated cresyl red ($CRBr_3$) have shown striking properties due to their better photochemical properties and lipophilicity which are important outcomes for photodynamic therapy (PDT) and photodynamic antimicrobial chemotherapy (PACT). These preliminary results suggest that the novel derivatives in comparison to the commercial dyes could be promising photosensitizers (PSs) for use in photodynamic therapy (PDT) and photodynamic antimicrobial chemotherapy (PACT).

4. Experimental details

4.1. Materials/chemicals

Cresyl violet (9-amino-5-imino-5*H*-benzo[α]phenoxazine) as an acetate salt was purchased from Sigma Chemical Co. (St. Louis, MO, Fluka Chemicals) (C1791-1G) No. CAS [10510-54-0] and purified by the methodology previously described.[5]

The solvents used were of analytical and HPLC grade. They were obtained from Cicarelli, Sintorgan and Anedra and used without further purification. All chemicals were of the highest

purity grade commercially available (Cicarelli, Sintorgan, Anedra). Solutions of bromo were prepared using molecular bromo (Carlo Erba) with a purity >99.9%. Aqueous solutions were prepared using ultrapure water from the Milli-Q® water purification system (Millipore Corporation, USA).

Thin-layer chromatography (TLC) was carried out using 250 μm silica gel plates (E. Merck) with chloroform : methanol (4 : 1 v : v) as the solvent system and the photographs were visually analyzed under daylight and UV light at λ = 254 nm. Deuterated dimethylsulfoxide (DMSO-d_6; purity >99.8%) was purchased from Sigma Chemical Co. (St. Louis, MO).

4.2. Instrumentation

Absorption spectra were recorded out at room temperature on a Varian Cary 50 UV-Visible spectrophotometer and a Shimadzu UV-2101 PC UV-Visible scanning spectrophotometer using 1 cm and 5 cm path length quartz cells, respectively.

NMR spectra were recorded on a Bruker AVANCE II 400 nuclear magnetic resonance spectrometer equipped with a 5 mm BBI 1H/D-BB ZGRD Z8202/0349 inverse probe and a variable temperature unit (VTU) (Bruker BioSpin, Billerica, MA) for ^{1}H and ^{13}C. The spectra were recorded at room temperature in DMSO-d_6. NMR spectra obtained at 0.05 M of the samples were manually phased, baseline corrected, and calibrated to the DMSO-d_6 residual solvent at 2.504 ppm, using the MestRe-C 4.9.9.6 software as a data processor.

Mass spectra were recorded in solid state on a Quadrupolar Finnigan 3300 F-100 mass spectrophotometer by electron ionization (EI-MS) at 70 eV. ESI high-resolution mass spectra (HRMS) were recorded on a Bruker Micro QTOF II spectrometer equipped with an ESI source, and the samples previously dissolved in HPLC grade methanol at a final concentration of 10 μg mL^{-1} were employed.

Fourier transform infrared (FT-IR) spectra were recorded in the range of 4000–600 cm^{-1} on a Nicolet 5SXC FT-IR spectrometer using KBr pellets.

Reversed-phase high-performance liquid chromatography (RP-HPLC) was carried out using an Agilent 1100 Series HPLC system (Agilent Technologies, Waldbronn, Germany) equipped with an isocratic pump, an autosampler, a column thermostat, and a UV-Vis spectrophotometric detector set at 280 nm, 510 nm and 590 nm. A reversed-phase C18 (Supelco®) column (4.6 mm × 250 mm, 5 μm) with a guard column and a flow rate of 1.0 mL min^{-1} were used. The column temperature was set at 25 °C in all cases and the injection volume was 20 μL. The chromatographic system was controlled by an Agilent ChemStation software package. The best chromatographic resolution was achieved by a mixture of methanol : aqueous solution of trimethylammonium phosphate 83 mM (80 : 20 v/v), which was prepared using ultrapure water from the Milli-Q® water purification system (Millipore Corporation, USA). The mobile phase and the samples prepared in the mobile phases were filtered through a Millipore® Type FH filter (0.45 μm pore size). Subsequently, the mobile phases were vacuum degassed. Data were produced by means of a Peak Simple Chromatography Data System®.

4.3 Synthesis

4.3.1. General aspects. The reaction progress and purity of the compounds were monitored by RP-HPLC and TLC. All the solutions were freshly prepared before being used. The reaction solvent was removed under reduced pressure and the solid residue was analyzed by RP-HPLC. During all the experiments, the reaction mixture was stirred and the round-bottom flask was protected from light.

Tribrominated cresyl violet ($CVBr_3$). In order to prepare $CVBr_3$, 15 mg (4.67×10^{-5} mol) of purified dye CV was dissolved in 20 mL of HPLC grade methanol, and then a solution of bromine in the same solvent (1.49×10^{-4} mol, 5 mL) was added dropwise with constant stirring. The reaction product was filtered through a Millipore® Type FH filter (0.45 μm pore size) and methanol was removed at 40 °C. The crude product did not need any further purification. The best reaction conditions were radio dye : bromine 1 : 3.2 at room temperature for 30 minutes (purity >98% by RP-HPLC).

IR (KBr, cm^{-1}). ν 1457 (N–H), 1315 (C–N), 1251, 1148, 1108 (C–H, N–H), 912, 770, 697 (oop C–H) t_R RP-HPLC (n = 7, min): 8.0 ± 0.6. R_f TLC (n = 7): 0.59 ± 0.03. ^{1}H-RMN (DMSO-d_6, 400.1 MHz): δ (ppm) = 7.94 (s, 1H), 8.04 (s, 1H), 8.29 (s, 1H), 8.74 (s, 2H). ^{13}C-RMN (DMSO-d_6, 100.6 MHz): δ (ppm) = 92.6, 94.9, 108.7, 123.7, 125.2, 125.9, 128.7, 130.2, 131.8, 133.6, 133.9, 137.3, 144.1, 149.5, 150.2, 160.0. EI-MS (70 eV, m/z): 498 $[M]^+$ 446, 419, 340, 281, 207. HRMS (ESI): calcd for $C_{17}H_{10}Br_3N_2O$ $[MH]^+$: 495.8296, $[MH + 2]^+$: 497.8275, $[MH + 4]^+$: 499.8255, $[MH + 6]^+$: 501.8234; found: 495.8304, 497.8291, 499.8273, 501.8218.

Tribrominated cresyl red ($CRBr_3$). In order to prepare $CRBr_3$, 15 mg (5.72×10^{-5} mol) of purified dye CR was dissolved in 20 mL of chloroform: methanol 7 : 3 v/v, and then a solution of bromine in the same system solvent (1.83×10^{-4} mol, 5 mL) was added dropwise with constant stirring. The reaction product was filtered through a Millipore® Type FH filter (0.45 μm pore size) and the medium was removed at 40 °C. The crude product did not need any further purification. The best reaction conditions were radio dye : bromine 1 : 3.2 at room temperature for 30 minutes (purity >98% by RP-HPLC).

IR (KBr, cm^{-1}). ν 1739 (C=O), 1457 (N–H), 1323 (C–N, C–N–H), 1259, 1092, 1022 (C–H, N–H) 797, 687 (oop C–H). t_R RP-HPLC (n = 7, min): 30 ± 2. R_f TLC (n = 7): 0.91 ± 0.06. ^{1}H-RMN (DMSO-d_6, 400.1 MHz): δ (ppm) = 6.98 (t, 1H), 7.91 (t, 1H), 8.17 (s, 1H), 8.32 (d, 1H), 8.68 (d, 1H). EI-MS (70 eV, m/z): 500 $[M]^+$ 446, 336, 284, 256, 207. HRMS (ESI): calcd for $C_{17}H_8Br_3NO_2$ $[MNa]^+$: 518.7950, $[MNa + 2]^+$: 520.7930, $[MNa + 4]^+$: 522.7909, $[MNa + 6]^+$: 524.7889; found: 518.7887, 520.7951, 522.7933, 524.7784.

4.4. Aggregation behaviour

4.4.1. Experimental aggregation in organic and aqueous solutions. Aggregation of CV, CR, $CVBr_3$ and $CRBr_3$ was studied by means of the spectral curves in ethanol and DMF as a

function of dye concentration (10^{-6} M to 10^{-4} M) between 200 and 800 nm. Stock solutions of dyes were freshly prepared in duplicate and then appropriately diluted with the same solvent. All experiments were carried out at least twice with consistent results.

Besides, the spectral curves of CV were recorded in water and water : polyethylene glycol (PEG) 400 75 : 25 v/v.

4.4.2. Computational details. Theoretical calculations were performed using the GAUSSIAN 03 suite of programs. All geometry optimizations were computed using the hybrid density functional B3LYP and the standard 6-31+G(d) basis set. The stationary points were located by the Berny algorithm using redundant internal coordinates. Analytical Hessians were computed to determine the nature of stationary points (one and zero imaginary frequencies for transition states and minima, respectively) and to calculate the unscaled zero-point energies (ZPEs) as well as the thermal corrections and entropy effects using the standard statistical mechanics relationships for an ideal gas. Non-specific solvent effects were described by using the self-consistent reaction field (SCRF) approach in Tomasi's formalism. Single point PCM [B3LYP/6-31+G(d)] calculations were performed to estimate the UV-spectral profile of the dyes.

4.5. Determination of log *P*

4.5.1. $\log P_{HPLC}$. The general procedure consisted of the measurement of the retention time under isocratic conditions with varying amounts of methanol like an organic modifier (φ).[27]

Methanol–buffer (pH 7.4) mixtures were used as mobile phases, with methanol contents between 65% and 90% v/v in 5% increments (final pH from 8.9 to 9.5). The buffer (pH 7.4, 10 mM) was prepared using potassium phosphate monobasic (19.7%) and sodium phosphate dibasic (80.3%) in Milli-Q® water.

Seven structurally related compounds were evaluated as references in order to establish the $\log P_{O/W} - \log k_w$ relationship, and their partition coefficient ($\log P_{O/W}$) values were taken from the literature to cover a wide range of lipophilicity (2.83–6.58) (Table 1).

A multi-wavelength UV-Visible detector was fixed at the λ_{max} of the compounds. The test substances and the reference compounds were injected into a column in triplicate.

The capacity factor (k') of all compounds was calculated from the experimentally determined retention data using eqn (3).

$$k' = (t_R - t_0)/t_0 \quad (3)$$

where t_R is the retention time of the solute and t_0 is the hold-up time (dead time) defined as the retention time of a non-retained compound; it was determined by injection of methanol.[51]

The log k' values were plotted against the volume percent of methanol in the eluent (φ) for each reference compound and the test substance based on the established linear relationship (eqn (4)), where S is the slope.

$$\log k' = S\varphi + \log k_w \quad (4)$$

The values of log k' corresponding to 100% aqueous solution (0% modifier) were obtained for each compound by means of extrapolation ($\log k_w$). In this case, k' was independent of the organic modifier effect, and the polar–non-polar partitioning was more similar to the shake measurements and dependent on the solute structure and polar functionalities.[52]

A log k_w *versus* $\log P_{O/W}$ plot (eqn (5)) was generated for the reference compounds.

$$\log P_{O/W} = a \log k_w - b \quad (5)$$

In the next step, the obtained coefficients a and b and the $\log k_w$ values of CR, $CVBr_3$ and $CRBr_3$ were used to calculate their partition coefficient ($\log P_{HPLC}$) using the eqn (6).

$$\log P_{HPLC} = a \log k_w - b \quad (6)$$

Regression and correlation analyses were performed using OriginPro 8 SR0 (OriginLab Corporation).

4.5.2. Theoretical calculation clog *P*. Different softwares allowed theoretical calculations of various lipophilicity descriptors on the basis of the obtained geometry of the molecule.[53]

For purposes of comparison, the theoretical partition coefficients (clog *P*) of the compounds were calculated by a fragment-based approach, employing the commercially available chemical software ACD/log *P* program Version 6.0 (Toronto, Canada) and freeware programs: Molinspiration Cheminformatics Software (milog *P* 2.2) and OSIRIS Property Explorer.

The correlation between the experimental data ($\log k_w$) and software-predicted lipophilicity (clog *P*) has been compared by linear regression analysis (eqn (7)) to determine the parameters of the relationship.

$$\text{clog } P = a \log k_w + b \quad (7)$$

4.6. Photodynamic properties: singlet oxygen determination

Solutions of CV, CR, $CVBr_3$ and $CRBr_3$ dyes were irradiated at 5 cm distance with a Parathom® lamp (OSRAM – 5 W) in 1 cm path length quartz cells with 9,10-dimethylanthracene (DMA, absorbance ~0.6) in DMF. To insure that in all experiments an equal number of photons were absorbed per unit time, the concentration for each dye was adjusted at an absorbance of ~0.18 at the λ_{max}. The kinetics of DMA photooxidation were studied by following the decrease of the absorbance (Abs) at λ_{max} = 378 nm as a function of irradiation time. The observed rate constants (k_{obs}) were obtained by a linear least-squares fit of the semilogarithmic Ln Abs_0/Abs *versus* time plot and the singlet oxygen quantum yields (Φ_Δs) were calculated relative to methylene blue dye used as a reference (MB, Φ_Δ = 1).

The Φ_Δs of the dyes were calculated using eqn (8), where PS is the photosensitizer, Ref is the reference compound and Abs_0 is the initial absorbance at 378 nm.

$$\Phi_\Delta^{PS} = \frac{\Phi_\Delta^{Ref} k_{obs}^{PS} Abs_0^{Ref}}{k_{obs}^{Ref} Abs_0^{PS}} \quad (8)$$

Acknowledgements

Financial support of this research from Secretaría de Ciencia y Técnica de la Universidad Nacional de Córdoba (SECYT-UNC, No. 162/12) and Fondo para la Investigación Científica y Tecnológica

(FONCYT, No. 109/08) of Argentina is gratefully acknowledged. The authors thank Dr Diego Andrada for theoretical calculations and helpful discussions. We wish to thank Dr Gloria Bonetto for developing the nuclear magnetic resonance spectra.

Notes and references

1 R. J. Nieckarz, J. Oomens, G. Berden, P. Sagulenko and R. Zenobi, *Phys. Chem. Chem. Phys.*, 2013, **15**, 5049–5056.
2 A. Jafari, A. Ghanadzadeh, H. Tajalli, M. Yeganeh and M. Moghadam, *Spectrochim. Acta, Part A*, 2007, **66**, 717–725.
3 D. Hazafy, M. V. Salvia, A. Mills, M. G. Hutchings, M. P. Evstigneev and J. A. Parkinson, *Dyes Pigm.*, 2011, **88**, 315–325.
4 S. J. Isak and E. M. Eyring, *J. Phys. Chem.*, 1992, **96**, 1738–1742.
5 M. N. Urrutia and C. S. Ortiz, *Biotech. Histochem.*, 2015, **90**, 159–166.
6 A. Master, M. Livingston and A. Sen Gupta, *J. Controlled Release*, 2013, **168**, 88–102.
7 E. Alves, M. A. Faustino, J. P. Tomé, M. G. Neves, A. C. Tomé, J. A. Cavaleiro, A. Cunha, N. C. Gomes and A. Almeida, *Bioorg. Med. Chem.*, 2013, **21**, 4311–4318.
8 C. A. Robertson, D. H. Evans and H. Abrahamse, *J. Photochem. Photobiol., B*, 2009, **96**, 1–8.
9 A. Hanakova, K. Bogdanova, K. Tomankova, K. Pizova, J. Malohlava, S. Binder, R. Bajgar, K. Langova, M. Kolar, J. Mosinger and H. Kolarova, *Microbiol. Res.*, 2014, **169**, 163–170.
10 N. Nishiyama, Y. Morimoto, W. D. Jang and K. Kataoka, *Adv. Drug Delivery Rev.*, 2009, **61**, 327–338.
11 F. C. Rossetti, L. B. Lopez, A. R. Carollo, J. A. Thomazini, A. C. Tedesco and M. V. Bentley, *J. Controlled Release*, 2011, **155**, 400–408.
12 A. Gorman, J. Killoran, C. O'Shea, T. Kenna, W. M. Gallagher and D. F. O'Shea, *J. Am. Chem. Soc.*, 2004, **126**, 10619–10631.
13 C. W. Lin, J. R. Shulok, Y. K. Wong, C. F. Schanbacher, L. Cincotta and J. W. Foley, *Cancer Res.*, 1991, **51**, 1109–1116.
14 A. Chakraborty, R. Adhikari and S. K. Saha, *J. Mol. Liq.*, 2011, **164**, 250–256.
15 M. K. Goftar, K. Moradi and N. M. Kor. Euro, *J. Exp. Biol.*, 2014, **4**, 72–81.
16 A. G. Gilani, M. Moghadam, S. E. Hosseini and M. S. Zakerhamidi, *Spectrochim. Acta, Part A*, 2011, **83**, 100–105.
17 O. Valdes-Aguilera and D. C. Neckers, *J. Phys. Chem.*, 1988, **92**, 4286–4289.
18 C. C. Chang, Y. T. Yang, J. C. Yang, H. D. Wu and T. Tsai, *Dyes Pigm.*, 2008, **79**, 170–175.
19 T. Nyokong, *Coord. Chem. Rev.*, 2007, **251**, 1707–1722.
20 O. Valdes-Aguilera and D. C. Neckers, *Acc. Chem. Res.*, 1989, **22**, 171–177.
21 S. D. Choudhury, A. C. Bhasikuttan, H. Pal and J. Mohanty, *Langmuir*, 2011, **27**, 12312–12321.
22 P. Zimcik, M. Miletin, Z. Musil, K. Kopecky, L. Kubza and D. Brault, *J. Photochem. Photobiol., A*, 2006, **183**, 59–69.
23 J. W. Millard, F. A. Alvarez-Núñez and S. H. Yalkowsky, *Int. J. Pharm.*, 2002, **245**, 153–166.
24 Z. Kabir-ud-Din Yaseen and M. S. Sheikh, *Colloids Surf., B*, 2011, **87**, 340–345.
25 A. Ghanadzadeh Gilani, M. Moghadama and M. S. Zakerhamidib, *Comput. Meth. Prog. Bio.*, 2011, **104**, 175–181.
26 K. Sztanke, W. Markowski, R. Swieboda and B. Polak, *Eur. J. Med. Chem.*, 2010, **45**, 2644–2649.
27 A. V. Rudraraju, P. N. A. Amoyaw, T. J. Hubin and M. O. F. Khan, *Pharmazie*, 2014, **69**, 655–662.
28 M. B. Spesia, D. Lazzeri, L. Pascual, M. Rovera and E. N. Durantini, *FEMS Immunol. Med. Microbiol.*, 2005, **44**, 289–295.
29 L. Cincotta, J. W. Foley and A. H. Cincotta, *Photochem. Photobiol.*, 1987, **46**, 751–758.
30 P. Zimcik, M. Miletin, H. Radilova, V. Novakova, K. Kopecky, J. Svec and E. Rudolf, *Photochem. Photobiol.*, 2010, **86**, 168–175.
31 A. R. Monahan and D. F. Blossey, *J. Phys. Chem.*, 1970, **74**, 4014–4021.
32 P. Dutta, R. Rai and S. Pandey, *J. Phys. Chem. B*, 2011, **115**, 3578–3587.
33 W. Leng and A. M. Kelley, *Langmuir*, 2003, **19**, 7049–7055.
34 M. Mirenda, M. G. Lagorio and E. San Román, *Langmuir*, 2004, **20**, 3690–3697.
35 A. R. Monahan, N. J. Germano and D. F. Blossey, *J. Phys. Chem.*, 1976, **76**, 1227–1233.
36 V. Kumar, G. A. Baker, S. Pandey, S. N. Baker and S. Pandey, *Langmuir*, 2011, **27**, 12884–12890.
37 P. Zimcik, M. Miletin, K. Kopecky, Z. Musil, P. Berka, V. Horakova, H. Kucerova, J. Zbytovska and D. Brault, *Photochem. Photobiol.*, 2007, **83**, 1497–1504.
38 M. Kostka, P. Zimcik, M. Miletin, P. Klemera, K. Kopecky and Z. Musil, *J. Photochem. Photobiol., A*, 2006, **178**, 16–25.
39 S. Bayar, H. A. Diner and E. Gonca, *Dyes Pigm.*, 2009, **80**, 156–162.
40 S. Wei, J. Zhou, D. Huang, X. Wang, B. Zhang and J. Shen, *Dyes Pigm.*, 2006, **71**, 61–67.
41 P. Zimcik, M. Miletin, J. Ponec, M. Kostka and Z. Fiedler, *J. Photochem. Photobiol., A*, 2003, **155**, 127–131.
42 D. Wróbel, A. Siejak and P. Siejak, *Sol. Energy Mater. Sol. Cells*, 2010, **94**, 492–500.
43 N. A. Kuznetsova, N. S. Gretsova, V. M. Derkacheva, S. A. Mikhalenko, L. I. Soloveva, O. A. Yuzhakova, O. L. Kaliya and E. A. Lukyanets, *Russ. J. Gen. Chem.*, 2002, **72**, 300–306.
44 V. T. Verdree, S. Pakhomov, G. Su, M. W. Allen, A. C. Countryman, R. P. Hammer and S. A. Soper, *J. Fluoresc.*, 2007, **17**, 547–563.
45 C. Johnson, S. B. Darling and Y. You, *Monatsh. Chem.*, 2011, **142**, 45–52.
46 S. R. Stoyanov, C. X. Yin, M. R. Gray, J. M. Stryker, S. Gusarov and A. Kovalenko, *J. Phys. Chem. B*, 2010, **114**, 2180–2188.
47 S. A. Gorman, A. L. Bell, J. Griffiths Dave Roberts and S. B. Brown, *Dyes Pigm.*, 2006, **71**, 153–160.

48 E. G. Friberg, B. Cunderlíková, E. O. Pettersen and J. Moan, *Cancer Lett.*, 2003, **195**, 73–80.
49 Z. Mrkvičková, P. Kovaříková, S. Balíková and J. Klimeš, *J. Pharm. Biomed. Anal.*, 2008, **48**, 310–314.
50 C. B. Nielsen, M. Johnsen, J. Arnbjerg, M. Pittelkow, S. P. McIlroy, P. R. Ogilby and M. Jørgensen, *J. Org. Chem.*, 2005, **70**, 7065–7079.
51 S. Ravetti, M. S. Gualdesi and M. C. Briñón, *J. Liq. Chromatogr. Relat. Technol.*, 2008, **3**, 1014–1032.
52 S. Griffin, S. Grant Wyllie and J. Markham, *J. Chromatogr. A*, 1999, **864**, 221–228.
53 D. Casoni, C. S. Cobzac and C. Sarbu, *Rev. Chim.*, 2010, **61**, 229–234.